

G-OFDM Variants Evaluation for Transmitter and Receiver Implementation

N.M.A.E.D. Wirastuti^{a,*}, J.M. Noras^b

^aDepartment of Electrical Engineering, Faculty of Engineering, Udayana University, Badung, 803611, Bali, Indonesia

^bFaculty of Engineering and Informatics, School of Electrical Engineering and Computer Science, University of Bradford, Bradford BD7 1DP, United Kingdom

Corresponding author: *dewi.wirastuti@umud.ac.id

Abstract— Orthogonal Frequency Division Multiplexing (OFDM) is chosen as a multiplexing technique and broadly used in today's radiocommunication environments to overcome spectrum insufficiency. In current OFDM applications, the IDFT/DFT algorithms are used for modulation and demodulation, efficiently implemented using the IFFT/FFT. The IFFT and FFT are some of the main components of OFDM systems, requiring intensive computation, especially for a high number of sub-channels. Reducing the computational burden of the IFFT/FFT would offer an advantage in reducing the total OFDM system complexity. In this proposed system, the idea of implementing the very fast Fourier transform (VFFT) in OFDM (later, it is called G-OFDM) is based on a trade-off between performance and complexity. The implementation complexity of G-OFDM is lower than OFDM. However, there is a performance cost. G-OFDM has been studied both analytically and in simulation over the AWGN channel. In particular, performance is marred by the non-uniformity of SNR among sub-carriers. In this study, it was proposed two G-OFDM variants called G1-OFDM and G2-OFDM. G1-OFDM is the least complex among all G-OFDM scenarios but gives the worst performance, while G2-OFDM gives the best performance but is the most complex. The results show that the performance of G-OFDM and its variants can be improved through the application of different values of n-quantization levels. In other words, using n-quantization levels, we can decrease the processing loss of the G system.

Keywords— Fast fourier transform; OFDM; AWGN channel; very fast fourier transform.

Manuscript received 30 Aug. 2020; revised 30 Dec. 2020; accepted 6 Apr. 2021. Date of publication 31 Aug. 2021. IJASEIT is licensed under a Creative Commons Attribution-Share Alike 4.0 International License.



I. INTRODUCTION

Communication system technology continues to develop to meet the need for high data rates. Orthogonal Frequency Division Multiplexing (OFDM) based on discrete Fourier transform (DFT) using a multicarrier modulation scheme (MCM) [1]. OFDM is the main competitor of the communication system needed for the next generation. This technology is remarkably interesting because it can still maintain its performance in poor channel conditions [2], [3]. So, OFDM has been widely used commercially and is still in research development, namely: Digital Video Broadcasting-Terrestrial (DVB-T) [4], Wireless Local Area Network (WLAN) [5], Broadband Wireless Access (BWA) especially IEEE 802.16d WiMAX [6], [7], IEEE 802.20 mobile Broadband Wireless Access (BWA) and Mobile Multimedia Access Communication (MMAC) [8]-[10] as well as 4th

Generation (4G) cellular standards such as Long Term Evolution (LTE) [11]-[14].

Since the pioneering work by Cooley and Turkey, an inordinate amount of work has been done on algorithms such as the radix-2m algorithm, Winograd algorithm, prime factor algorithm, and split radix algorithm. The very fast Fourier transform (VFFT) was introduced to reduce the implementation complexity of the fast Fourier transform (FFT) [15]. It has beneficial computational advantages over the ubiquitous FFT. Currently, several low-complexity techniques for computing Discrete Fourier transform (DFT), or inverse DFT exist, the latest of which is the VFFT algorithms considered in this paper.

Low-complexity techniques for DFT computation are useful in OFDM because they offer lower power consumption. Research of various algorithms on computational complexity reduction in OFDM has been investigating. The performance of Discrete Wavelet Transform (DWT), Double Density Discrete Wavelet Transforms (DDDWT), Discrete Cosine

Transform (DCT) that applied to OFDM have been studied in [17]-[24]. Also, the use of various FFT algorithms as 2-radix FFT, 4-radix FFT, Winograd FFT, and the very recent very fast Fourier transform (VFFT) in the OFDM system have been examined in [25]-[29].

We have investigated the implementation of an inverse VFFT and a VFFT algorithm in OFDM systems, using the G matrix, an integer form of the Fourier matrix [29]. The numbers of non-trivial multiplications of direct DFT and VFFT calculations, for various matrix dimensions N , using the G matrix, require appreciably fewer complex multiplications than using the Fourier matrix when $N \geq 16$. The VFFT algorithm is implemented in the OFDM system by replacing the IFFT/FFT with the IVFFT/VFFT, at transmitter and receiver, respectively. The IVFFT/VFFT is a linear process and completely reversible. The data was returned to the original input, whether we applied the IVFFT or VFFT in the transmitter, if we did the reverse in the receiver, i.e., $\mathbf{G}^{-1}\mathbf{G} = \mathbf{G}\mathbf{G}^{-1} = \mathbf{I}$.

In this paper, two different implementation variants are analyzed: G1-OFDM and G2-OFDM. The G1-OFDM model is the simplest compared to other G-OFDM variants. Both transmitter and receiver use a simple matrix, \mathbf{G}^* and \mathbf{G} . However, neither of these matrices satisfy the matched linear transform condition, i.e., $\mathbf{G}^*\mathbf{G} \neq \mathbf{I}$. For G2-OFDM, it satisfies the matched linear transform condition, i.e., $\mathbf{H}\mathbf{G}^*\mathbf{H}_2\tilde{\mathbf{H}}_1\mathbf{G} = \mathbf{I}$. The author explains the block diagrams of the proposed system in section II. Simulation results are discussed in Section III. Finally, the author presents the conclusion in section IV.

II. MATERIAL AND METHOD

The application of the G-OFDM variants model and row-gain characteristics in each transmitter and receiver part is proposed. We consider expanding our work by applying the conjugate G and G matrix to the OFDM transmitter and receiver, respectively, with lower computational complexity than the inverse G and G matrix in the OFDM transmitter and receiver. This is just one VFFT variant that can be applied to an OFDM system. Other G-OFDM variants are also presented in detail in this section.

The distinction between G-OFDM and its variants is in the way of implementing the G matrix (\mathbf{G}), the G approximation matrix ($\tilde{\mathbf{G}}$), correction factors (\mathbf{H}) and correction factor approximations ($\tilde{\mathbf{H}}_1$), for approximating the inverse Fourier (\mathbf{F}^{-1}) and Fourier matrix (\mathbf{F}), at the transmitter and receiver of the OFDM system, respectively. Consequently, we review some alternatives to the simpler implementation technique of the G system at the mobile transmitter and receiver. The utility of these implementation techniques can be studied by observing the row-gain characteristics of each model. The following assumptions have been made in analyzing our model, which is: the channel is assumed to be a perfect channel with AWGN, in use of matrix operations,

1. $\mathbf{G} = \text{round}(\mathbf{F})$,
2. $\mathbf{G}^* = \frac{\text{conj}(\mathbf{G})}{N}$; where N defines N -point FFT,
3. $\tilde{\mathbf{G}} = \frac{\text{round}(n\mathbf{G}\times\mathbf{F})}{n\mathbf{G}}$; where $n\mathbf{G}$ is the G matrix quantization level, $n\mathbf{G} \geq 2^n$, $n = 1,2,3,4,\dots,14$,
4. $\mathbf{H} = \mathbf{G}\mathbf{F}^{-1}$, where \mathbf{F}^{-1} defines the inverse Fourier matrix,

5. $\mathbf{H} = \mathbf{H}_2\tilde{\mathbf{H}}_1$, $\tilde{\mathbf{H}}_1 = \frac{\text{round}(n\mathbf{H}\times\mathbf{H})}{n\mathbf{H}}$; where $n\mathbf{H}$ is the H matrix quantization level, $n\mathbf{H} \geq 2^n$, $n = 1,2,3,4,\dots,14$, and $\mathbf{H}_2 = \mathbf{H}\{\tilde{\mathbf{H}}_1\}^{-1}$.

A. G-OFDM Model

A transformed discrete baseband G-OFDM system is illustrated in Figure 1 using matrix operations.

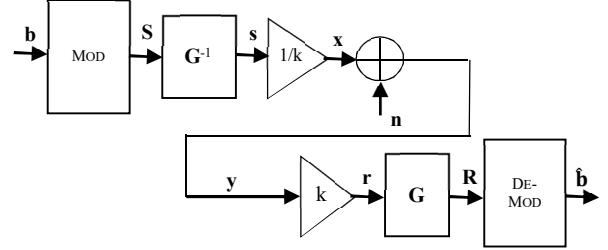


Fig. 1 G-OFDM model

Information bits in a series form which denoted as $b \in b_i^{1 \times N}$ is converted into M-ary symbols in parallel data. These symbols then are transmitted on N sub-channels, denoted $s \in s_i^{N \times 1}$. The type of modulation used determines the number of bits per sub-carrier. The number of information bits per G-OFDM symbol depends on the number of sub-carriers N . Each sub-carrier transmits one modulation symbol during each G-OFDM symbol. The output of the inverse G block represents the G-OFDM symbol with N samples in the time domain. Thus, we have

$$\mathbf{s} = \mathbf{G}^{-1}\mathbf{S}, \quad (1)$$

\mathbf{G}^{-1} is the $N \times N$ inverse G matrix with rational number entries since the inverse matrix is derived from the ratio of adjoint and determinant matrix. The time-domain sampled signal vector, \mathbf{s} , is normalized by a factor of $1/k$ by referring the total transmitted signal power to 1 watt. The normalized signal transmission, $\mathbf{x} = (1/k)\mathbf{G}^{-1}\mathbf{S}$, is sent sequentially through the channel. The channel is assumed to be perfect, but with AWGN. The AWGN time vector is denoted as

$$\mathbf{n} = \mathbf{F}^{-1}\mathbf{N} \quad (2)$$

The received signal is obtained as:

$$\mathbf{y} = \mathbf{x} + \mathbf{n}, \quad (3)$$

$$\mathbf{y} = (1/k)\mathbf{G}^{-1}\mathbf{S} + \mathbf{F}^{-1}\mathbf{N}, \quad (4)$$

$1/k$ denotes the transmitted signal normalization factor and \mathbf{F}^{-1} is the inverse Fourier matrix. For a fair comparison, the factor $1/k$ normalizes the G-OFDM transmitted signal power to have the same transmitted signal power as OFDM. The normalized factor can be computed as:

$$\frac{1}{k} = \frac{\sum_{j=0}^{N-1} \sum_{i=0}^{N-1} |F_{ij}|^{-1}|^2}{\sum_{j=0}^{N-1} \sum_{i=0}^{N-1} |G_{ij}|^{-1}|^2} \quad (5)$$

Then we have the received signal vector after de-

normalization by the factor k :

$$\mathbf{r} = k((1/k)\mathbf{G}^{-1}\mathbf{S} + \mathbf{F}^{-1}\mathbf{N}), \quad (6)$$

$$\mathbf{r} = \mathbf{G}^{-1}\mathbf{S} + (k)\mathbf{F}^{-1}\mathbf{N}. \quad (7)$$

In the receiver, the processing of the transmitted signal gives the received signal in the frequency domain as

$$\mathbf{R} = \mathbf{G}(\mathbf{G}^{-1}\mathbf{S} + (k)\mathbf{F}^{-1}\mathbf{N}), \quad (8)$$

which simplifies to

$$\mathbf{R} = \mathbf{S} + (k)\mathbf{G}\mathbf{F}^{-1}\mathbf{N}. \quad (9)$$

The received signal vector, \mathbf{R} , is then demodulated, and we recover data as $\hat{\mathbf{b}} \in \hat{\mathbf{b}}_i^{1 \times N}$.

In the extended G-OFDM model, we apply the inverse $\tilde{\mathbf{G}}$ approximation matrix $\tilde{\mathbf{G}}^{-1}$ and the $\tilde{\mathbf{G}}$ approximation matrix $\tilde{\mathbf{G}}$ at transmitter and receiver, respectively, as shown in Figure 2. With the same assumptions and analysis applied to the extended system, the properties of G-OFDM with $\tilde{\mathbf{G}}$ and $\tilde{\mathbf{G}}^{-1}$ implementation are summarised as follows:

1. The output of $\tilde{\mathbf{G}}^{-1}$ block, \mathbf{s} :

$$\mathbf{s} = \tilde{\mathbf{G}}^{-1}\mathbf{S} \quad (10)$$

2. Transmitted signal vector after normalization, \mathbf{x} :

$$\mathbf{x} = \left(\frac{1}{k}\right)\tilde{\mathbf{G}}^{-1}\mathbf{S} \quad (11)$$

3. Received signal vector, \mathbf{y} :

$$\mathbf{y} = \left(\frac{1}{k}\right)\tilde{\mathbf{G}}^{-1}\mathbf{S} + \mathbf{F}^{-1}\mathbf{N} \quad (12)$$

4. Received signal vector after de-normalization, \mathbf{r} :

$$\mathbf{r} = \tilde{\mathbf{G}}^{-1}\mathbf{S} + (k)\mathbf{F}^{-1}\mathbf{N} \quad (13)$$

5. Received signal vector in the frequency domain, \mathbf{R} :

$$\mathbf{R} = \mathbf{S} + (k)\tilde{\mathbf{G}}\mathbf{F}^{-1}\mathbf{N} \quad (14)$$

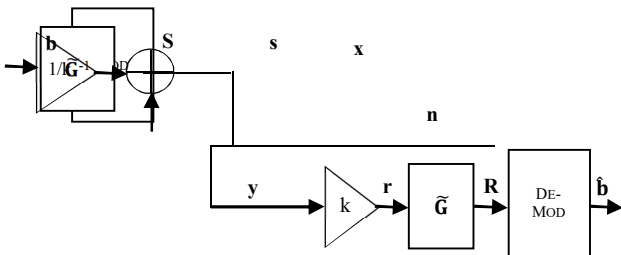


Fig. 2 G-OFDM model with $\tilde{\mathbf{G}}$ implementation

B. G-OFDM Variants

G-OFDM variants arise from different combinations of \mathbf{G} matrix, \mathbf{G} , and or \mathbf{G} approximation matrix $\tilde{\mathbf{G}}$, and multiplicative correction factor, \mathbf{H} , applied to OFDM systems. In other words, various approximations for the inverse Fourier

and Fourier matrices are used at transmitter and receiver. The following G-OFDM variants are explained, as shown below:

1) *G1-OFDM Model*: A variant of the G-OFDM system, which we call G1-OFDM, can be seen in Figure 3. The \mathbf{G}^* frame's output represents the N samples of the G2-OFDM symbol in the time domain. Hence, we have

$$\mathbf{s} = \mathbf{G}^*\mathbf{S}, \quad (15)$$

Where \mathbf{G}^* denotes the conjugate \mathbf{G} matrix with $\{0, \pm 1, \pm j, \pm 1 \pm j\}$ entries, and \mathbf{S} is the transmitted signal before normalization. After normalization, \mathbf{S} can be written as:

$$\mathbf{x} = (1/k)\mathbf{G}^*\mathbf{S} \quad (16)$$

The received data, \mathbf{y} , is the summation of the normalized signal vector with noise vector, can be written as:

$$\mathbf{y} = (1/k)\mathbf{G}^*\mathbf{S} + \mathbf{F}^{-1}\mathbf{N} \quad (17)$$

After de-normalization, it can be shown as:

$$\mathbf{r} = k((1/k)\mathbf{G}^*\mathbf{S} + \mathbf{F}^{-1}\mathbf{N}), \quad (18)$$

$$\mathbf{r} = \mathbf{G}^*\mathbf{S} + (k)\mathbf{F}^{-1}\mathbf{N}, \quad (19)$$

After passing the \mathbf{G} block, the received signal is obtained:

$$\mathbf{R} = \mathbf{G}(\mathbf{G}^*\mathbf{S} + (k)\mathbf{F}^{-1}\mathbf{N}), \quad (20)$$

$$\mathbf{R} = \mathbf{G}\mathbf{G}^*\mathbf{S} + (k)\mathbf{G}\mathbf{F}^{-1}\mathbf{N}. \quad (21)$$

The normalization factor $1/k$ for this model can be written as:

$$\frac{1}{k} = \frac{\sum_{j=0}^{N-1} \sum_{i=0}^{N-1} |F_{ij}^{-1}|^2}{\sum_{j=0}^{N-1} \sum_{i=0}^{N-1} |G_{ij}|^2}. \quad (22)$$

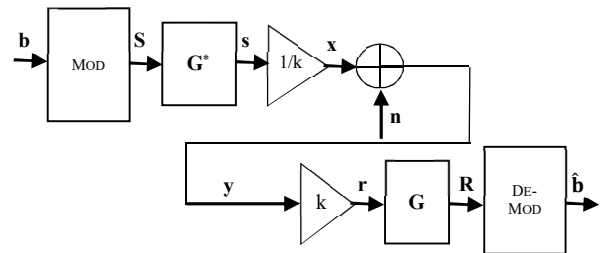


Fig. 3 G1-OFDM model

The extended model is created by applying $\tilde{\mathbf{G}}$ in the G1-OFDM model, as illustrated in Figure 4. The G1-OFDM with applied $\tilde{\mathbf{G}}$ has properties that can be summarised:

1. The output of the $\tilde{\mathbf{G}}^*$ block, \mathbf{s} :

$$\mathbf{s} = \tilde{\mathbf{G}}^*\mathbf{S}; \quad (23)$$

2. Transmitted signal vector after normalization, \mathbf{x} :

$$\mathbf{x} = \left(\frac{1}{k}\right)\tilde{\mathbf{G}}^*\mathbf{S}; \quad (24)$$

3. Received signal vector, \mathbf{y} :

$$\mathbf{y} = \left(\frac{1}{k}\right) \tilde{\mathbf{G}}^* \mathbf{S} + \mathbf{F}^{-1} \mathbf{N}; \quad (25)$$

4. Received signal vector after de-normalization, \mathbf{r} :

$$\mathbf{r} = \tilde{\mathbf{G}}^* \mathbf{S} + (k) \mathbf{F}^{-1} \mathbf{N}; \quad (26)$$

5. Received signal vector in the frequency domain, \mathbf{R} :

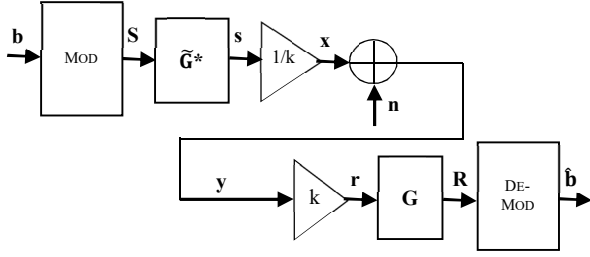


Fig. 4 G1-OFDM model with $\tilde{\mathbf{G}}$ implementation

2) *G2-OFDM Model*: A transformed discrete baseband G2-OFDM system using matrix operations is illustrated in Figure 5. The G2-OFDM properties can be summarized as follows:

1. The output of the $\mathbf{HG}^* \mathbf{H}_2$ block, \mathbf{s} :

$$\mathbf{s} = \mathbf{HG}^* \mathbf{H}_2 \mathbf{S}; \quad (28)$$

2. Transmitted signal vector after normalization, \mathbf{x} :

$$\mathbf{x} = \left(\frac{1}{k}\right) \mathbf{HG}^* \mathbf{H}_2 \mathbf{S}; \quad (29)$$

3. Received signal vector, \mathbf{y} :

$$\mathbf{y} = \left(\frac{1}{k}\right) \mathbf{HG}^* \mathbf{H}_2 \mathbf{S} + \mathbf{F}^{-1} \mathbf{N}; \quad (30)$$

4. Received signal vector after de-normalization, \mathbf{r} :

$$\mathbf{r} = \mathbf{HG}^* \mathbf{H}_2 \mathbf{S} + (k) \mathbf{F}^{-1} \mathbf{N}; \quad (31)$$

5. Received signal vector in the frequency domain, \mathbf{R} :

$$\mathbf{R} = \tilde{\mathbf{H}}_1 \tilde{\mathbf{G}} \mathbf{HG}^* \mathbf{H}_2 \mathbf{S} + (k) \tilde{\mathbf{H}}_1 \tilde{\mathbf{G}} \mathbf{F}^{-1} \mathbf{N}. \quad (32)$$

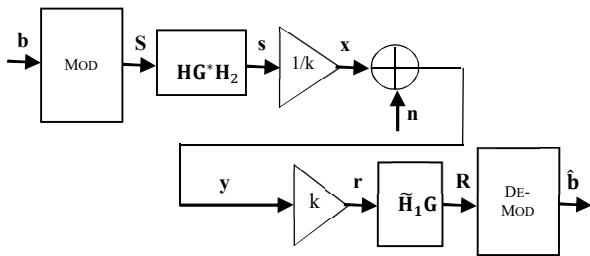


Fig. 5 G2-OFDM Model

Next, we replace \mathbf{G} and \mathbf{H} and apply $\tilde{\mathbf{G}}$, $\tilde{\mathbf{H}}_1$ and \mathbf{H}_2 in the model, to extend the G2-OFDM model as presented in Figure 6. The G2-OFDM with applied $\tilde{\mathbf{G}}$, $\tilde{\mathbf{H}}_1$ and \mathbf{H}_2 has properties:

6. The output of the $\mathbf{HG}^* \mathbf{H}_2$ block, \mathbf{s} :

$$\mathbf{s} = \mathbf{HG}^* \mathbf{H}_2 \mathbf{S}; \quad (32)$$

7. Transmitted signal vector after normalization, \mathbf{x} :

$$\mathbf{x} = \left(\frac{1}{k}\right) \mathbf{HG}^* \mathbf{H}_2 \mathbf{S}; \quad (33)$$

8. Received signal vector, \mathbf{y} :

$$\mathbf{y} = \left(\frac{1}{k}\right) \mathbf{HG}^* \mathbf{H}_2 \mathbf{S} + \mathbf{F}^{-1} \mathbf{N}; \quad (34)$$

9. Received signal vector after de-normalization, \mathbf{r} :

$$\mathbf{y} = \mathbf{HG}^* \mathbf{H}_2 \mathbf{S} + (k) \mathbf{F}^{-1} \mathbf{N}; \quad (35)$$

10. Received signal vector in the frequency domain, \mathbf{R} :

$$\mathbf{R} = \tilde{\mathbf{H}}_1 \tilde{\mathbf{G}} \mathbf{HG}^* \mathbf{H}_2 \mathbf{S} + (k) \tilde{\mathbf{H}}_1 \tilde{\mathbf{G}} \mathbf{F}^{-1} \mathbf{N}. \quad (36)$$

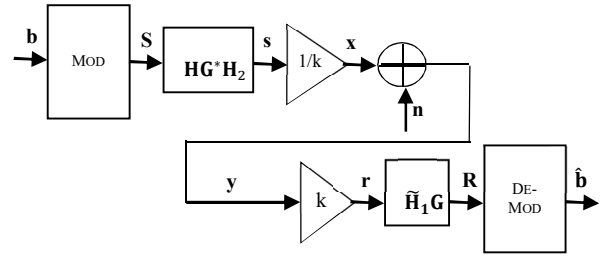


Fig. 6 G2-OFDM model with applied $\tilde{\mathbf{G}}$, $\tilde{\mathbf{H}}_1$ and \mathbf{H}_2

C. Processing Gain/Loss of G-OFDM

Since data are transmitted using \mathbf{G}^{-1} , the total transmitted signal power would be typically less than 1,

$$S_{inv}(G) = \sum_i \sum_j |G_{ij}^{-1}|^2 < 1, \quad (37)$$

At the receiver, using \mathbf{G} to process the data, the signal power would be typically higher than 1, so:

$$S(G) = \sum_i \sum_j |G_{ij}^{-1}|^2 > 1. \quad (38)$$

The signal power that we get after \mathbf{G} processing would be unity, since $\mathbf{G}^{-1} \mathbf{G} = \mathbf{I}$. Ideally, all sub-channels of a transmission system should have the same BER performance for the same E_b/N_0 into the decision circuit (assuming that noise is Gaussian PDF) here, whether \mathbf{F} or \mathbf{G} is being used for determining the E_b/N_0 required to get the same BER. The gain or loss of the \mathbf{G} processing technique is the difference of E_b/N_0 , and this is analyzed and simulated for the G-OFDM system and its variants.

The non-uniform row-gain of the \mathbf{G} matrix leads to a non-uniform noise contribution to the SNR of each subcarrier in the proposed system. This small non-uniform variation gives an almost uniform or flat noise power spectrum, with increased noise power compared to OFDM.

The processing gain/loss between G-OFDM and OFDM system in AWGN channel and without other impairments is defined by the factor:

$$\frac{\left\langle \sum_{j=0}^{N-1} |n_j|^2 \right\rangle}{\left\langle |k|^2 \sum_{j=0}^{N-1} |B_{ij} n_j|^2 \right\rangle} \quad (39)$$

Various approximations $\tilde{\mathbf{G}}_n$ for the 8-point G matrix can be seen as follows.

If $n = 1$

$$\tilde{\mathbf{G}}_1 = \begin{bmatrix} 1 & 1 & 1 & 1 & 1 & 1 & 1 & 1 \\ 1 & 1-j & -j & -1-j & -1 & -1+j & j & 1+j \\ 1 & -j & -1 & j & 1 & -j & -1 & j \\ 1 & -1-j & j & 1-j & -1 & 1+j & -j & -1+j \\ 1 & -1 & 1 & -1 & 1 & -1 & 1 & -1 \\ 1 & -1+j & -j & 1+j & -1 & 1-j & j & -1-j \\ 1 & j & -1 & -j & 1 & j & -1 & -j \\ 1 & 1+j & j & -1+j & -1 & -1-j & -j & 1-j \end{bmatrix} = \mathbf{G};$$

If $n = 2$

$$\tilde{\mathbf{G}}_2 = \begin{bmatrix} 1 & 1 & 1 & 1 & 1 & 1 & 1 & 1 \\ 1 & 0.5 - 0.5j & -j & -0.5 - 0.5j & -1 & -0.5 + 0.5j & j & 0.5 + 0.5j \\ 1 & -j & -1 & j & 1 & -j & -1 & j \\ 1 & -0.5 - 0.5j & j & 0.5 - 0.5j & -1 & 0.5 + 0.5j & -j & -0.5 + 0.5j \\ 1 & -1 & 1 & -1 & 1 & -1 & 1 & -1 \\ 1 & -0.5 + 0.5j & -j & 0.5 + 0.5j & -1 & 0.5 - 0.5j & j & -0.5 - 0.5j \\ 1 & j & -1 & -j & 1 & j & -1 & -j \\ 1 & 0.5 + 0.5j & j & -0.5 + 0.5j & -1 & -0.5 - 0.5j & -j & 0.5 - 0.5j \end{bmatrix}$$

D. Row-gain Matrix Characteristics Constructed Tx and Rx

The non-uniform row-gain of the G matrix is a potential problem for implementation. For the Fourier matrix suitably normalized, the row-gain is equal to one (unity) for all rows, whereas, for G, it is not necessarily unity. This section presents the row-gains distribution of applied matrices at transmitter and receiver, respectively, for G-OFDM and its variants. The matrices found within the transmitter and receiver in each model can be summarized as in Table 1.

TABLE I
APPLIED MATRICES IN G-OFDM AND ITS VARIANTS

Models	Tx	Rx
G-OFDM	$\mathbf{G}^{-1} = \mathbf{G1}$	$\mathbf{G} = \mathbf{G2}$
G-OFDM with applied $\tilde{\mathbf{G}}$	$\tilde{\mathbf{G}}^{-1}$	$\tilde{\mathbf{G}}$
G1-OFDM	\mathbf{G}^*	\mathbf{G}
G1-OFDM with applied $\tilde{\mathbf{G}}$	$\tilde{\mathbf{G}}^*$	$\tilde{\mathbf{G}}$
G2-OFDM	$\mathbf{HG}^* \mathbf{H}_2$	$\tilde{\mathbf{H}}_1 \mathbf{G}$
G2-OFDM with applied $\tilde{\mathbf{G}}, \tilde{\mathbf{H}}_1$ and $\tilde{\mathbf{H}}_2$	$\mathbf{H}\tilde{\mathbf{G}}^* \mathbf{H}_2 = \mathbf{G3}$	$\tilde{\mathbf{H}}_1 \tilde{\mathbf{G}} = \mathbf{G4}$

For example, to observe the row-gain distribution of G-OFDM and G2-OFDM with applied $\tilde{\mathbf{G}}, \tilde{\mathbf{H}}_1$ and $\tilde{\mathbf{H}}_2$ models, for later convenience, we specify the matrix in the transmitter and receiver as $\mathbf{G1}, \mathbf{G2}, \mathbf{G3}$ and $\mathbf{G4}$. The row-gain matrix distribution of G1 and G2 can be seen in Table 2 and 3, respectively. Afterward, the row-gain distributions of G3 and G4 are investigated in three different conditions, namely for $nG = nH, nG > nH$ and $nG < nH$. We define the row-gain of the i^{th} row G matrix as

$$B_j = \frac{\sum_i |G_{ij}|^2}{N} = [b_1 \quad b_2 \quad \dots \quad b_N], \quad (40)$$

$b_1 \quad b_2 \quad \dots \quad b_N$ Are not necessarily unity, i.e., non-uniform. With n-level quantization, the G matrix leads to the G approximation matrix, $\tilde{\mathbf{G}}$, which has $\{0, \pm 1, \pm \frac{1}{4}, \pm \frac{1}{2}, \dots, \pm j, \pm j \frac{1}{4}, \pm 1 \pm j, \pm \frac{1}{4} \pm j \frac{1}{4}, \dots\}$ entries. Alternatively, we can say the G approximation matrix is an approximate form of the F matrix. By using progressively higher n-level quantization, it will more closely approximate the Fourier matrix. Thus, various approximations $\tilde{\mathbf{G}}_n$ have

been developed to minimize the non-uniformity of the row-gain of the G matrix, which can be obtained by

$$\tilde{\mathbf{G}} = \frac{\mathbf{\Omega}}{n}, \quad (41)$$

Where $\mathbf{\Omega} = (n \times \mathbf{F})$; $n = 2^x$, n defines the quantization level, x is an integer, F is the Fourier matrix, and $\mathbf{\Omega}$ defines the degree of rounding, the n-quantization level of the Fourier matrix.

TABLE II
G1 ROW-GAIN DISTRIBUTIONS

Quantization level, nG	Gains	Number of occurrences of each value
1	1.0000	8
	1.1430	8
	1.1950	16
	1.2970	32

TABLE III
G2 ROW-GAIN DISTRIBUTIONS

Quantization level, nG	Gains	Number of occurrences of each value
1	1.0000	4
	1.1890	4
	1.2610	8
	1.3740	16
	1.4560	32

III. RESULTS AND DISCUSSION

In this work, the simulation was carried to assess the performance of the proposed system. The constellation diagram and Eb/No vs BER were the performance metrics used in this work. The parameter used in the simulation can be seen in Table 4. The performance of the proposed system was compared to conventional OFDM.

TABLE IV
PARAMETERS SIMULATION

Parameter	Value
FFT size	64
Modulation	QPSK
Eb/No	Range: 0 to 10 dB
Number of pilot sub-carriers (NSP)	4
Number of data sub-carriers (NSD)	48
Total number of sub-carriers (NST)	52
Useful symbol part (NU)	64
Number of a cyclic prefix (NCP)	16
Total sub-carriers on each OFDM symbol (NT)	80
Useful symbol part duration (TU)	3.2 μs
Cyclic prefix duration (TCP)	0.8 μs
OFDM symbol duration (TS)	4 μs

A. Constellation Diagram

The constellation diagrams presented in this section illustrate the G-OFDM model's behavior and its variants and are compared to OFDM constellation diagrams. The diagrams depict the received signal constellation. Figure 7 illustrates the constellation of OFDM received signals with QPSK modulation and Eb/No = 15 dB, 20 dB and 25 dB.

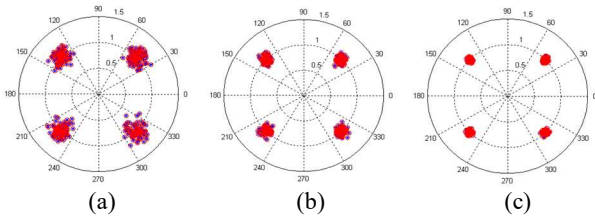


Fig. 7 OFDM received signals (a) $E_b/N_0=15$ dB, (b) $E_b/N_0=20$ dB, (c) $E_b/N_0=25$ dB

Figures 8 – 11 show received signals for G-OFDM and G-OFDM variants with QPSK modulation and $E_b/N_0 = 15$ dB, 20dB, and 25 dB.

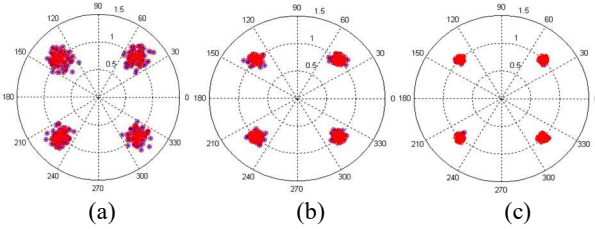


Fig. 8 G-OFDM received signals (a) $E_b/N_0=15$ dB, (b) $E_b/N_0=20$ dB, (c) $E_b/N_0=25$ dB.

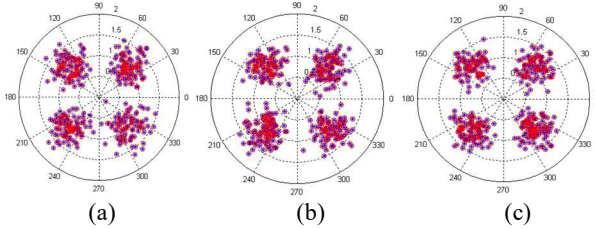


Fig. 9 G1-OFDM received signals (a) $E_b/N_0=15$ dB, (b) $E_b/N_0=20$ dB, (c) $E_b/N_0=25$ dB.

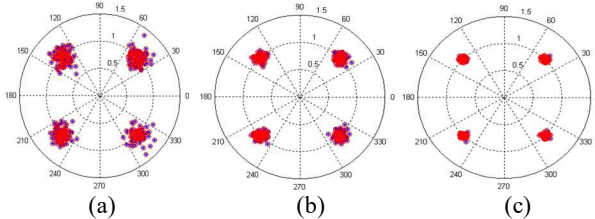


Fig. 10 G2-OFDM received signals (a) $E_b/N_0=15$ dB, (b) $E_b/N_0=20$ dB, (c) $E_b/N_0=25$ dB.

We see that simulated G-OFDM, G2-OFDM constellation diagrams with QPSK modulation in an AWGN channel are in perfect accordance with the simulated OFDM QPSK modulation constellation diagram. On the other hand, a simulated G1-OFDM constellation diagram seems more inadequate than a simulated OFDM constellation diagram. The system models (G matrix and H matrix in these models) introduce noise to the system. It is apparent from the constellation that the impairments that induce amplitude changes can move a symbol from its ideal location far enough to cross the rectangular boundary, resulting in a symbol error. These impairments will cause a broader spread of the received symbol around the ideal constellation point, making it more susceptible to detection error.

B. BER vs E_b/N_0 Performance under AWGN Channel

Simulations have been performed to evaluate and compare the G-OFDM and OFDM systems' performance over AWGN

channels. To have a fair comparison, we have normalized the transmitted signal of the G-system to 1 watt.

1) *G1-OFDM Model*: Figure 11 presents G-OFDM's BER performance, with three different level quantization ($n=2,4,8$) of the extended G-OFDM system, which is then compared to the BER performance of OFDM. At a BER of 10^{-3} , there is about 0.0001 dB relative processing loss using a quantization level $n=4$. For $n=8$, the performance is similar to OFDM, i.e., BER of 10^{-3} , $E_b/N_0=7.75$ dB. At the same BER, the performance for $n=2$ does not differ much from the system without quantization level ($n=1$) that is approximately about 8.5 dB and 8.45 dB. That means the relative processing loss for G-OFDM ($n=1$) is about 0.75 dB. By using $n=2$, the relative processing loss is about 0.70 dB. Thus, the system with $n=8$ and more gives an identical performance with OFDM.

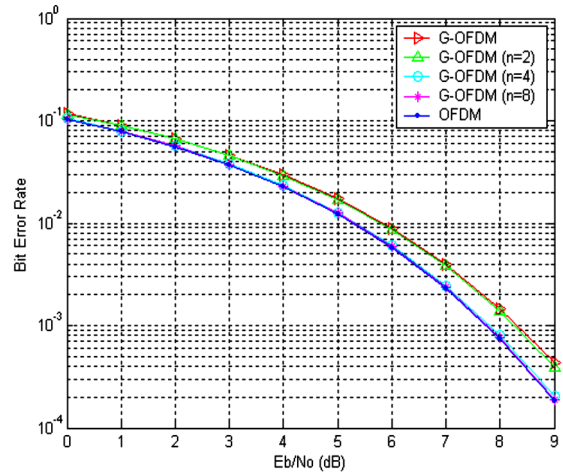


Fig. 11 G-OFDM performance with three different values of quantization levels, $n=2,4,8$.

2) *G1-OFDM Model*: In Figure 12, the BER vs E_b/N_0 performance of G1-OFDM is considered for five different values of quantization levels, $n=2,4,8,16,32$, also compared to OFDM. At a BER of 10^{-2} , the relative processing loss for the system without quantization level ($n=1$) is about 2.8 dB. With fairly rough quantization levels $n=2,4,8,16$, the relative processing loss is about 2.1 dB, 0.25 dB, 0.15 dB, 0.01 dB, respectively. The G1-OFDM begins to be quite similar in performance to OFDM when using $n=16$. With $n=32$, the model is very close in performance to OFDM.

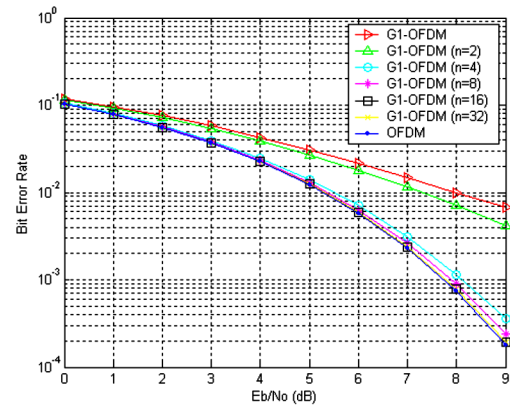
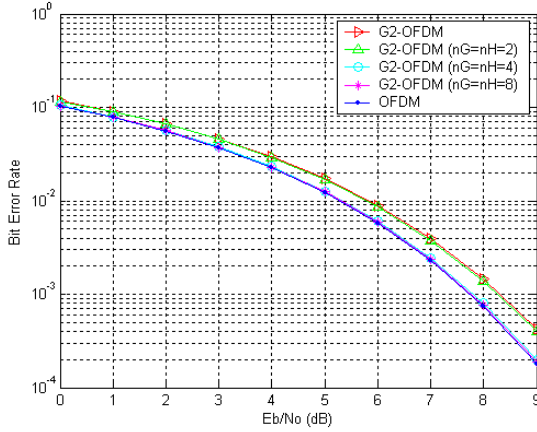
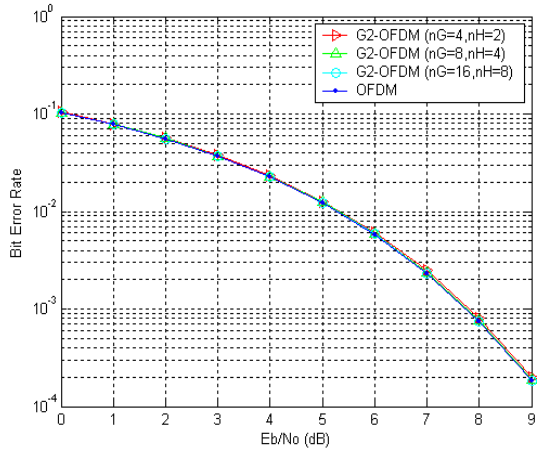


Fig. 12 G1-OFDM performance with three different values of quantization levels, $n=2,4,8,16,32$.

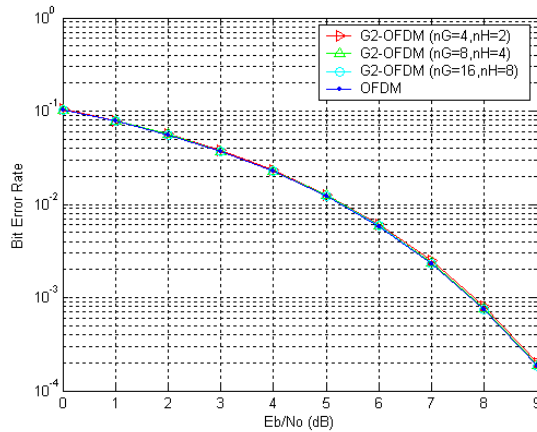
3) *G2-OFDM Model*: The performance of G2-OFDM and its extended schemes are investigated in three different conditions, which are for $nG=nH$, $nG>nH$ and $nG<nH$. Figure 13 presents the BER vs E_b/N_0 performance of G2-OFDM with QPSK modulation for $nG=nH$, $nG>nH$ and $nG<nH$. For $nG>nH$, the performance is explored in two circumstances: (a) different values of nG and nH : ($\{nG=4, nH=8\}$, $\{nG=8, nH=16\}$ and $\{nG=16, nH=8\}$). (b) different values of nG : ($n=4, 8, 16$) and nH is fixed: ($nH=2$). Also for $nG<nH$, two states are considered which are (a) nG fixed: ($nG=2$) and nH varies: ($nH=4, 8, 16, 32$), (b) nG and nH vary: ($\{nG=2, nH=4\}$, $\{nG=4, nH=8\}$, $\{nG=8, nH=16\}$ and $\{nG=16, nH=32\}$).



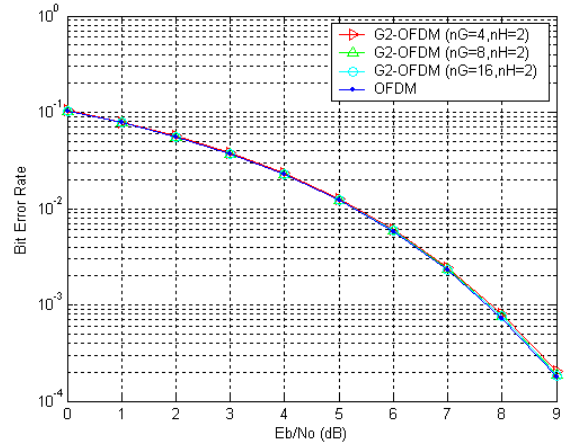
(a)



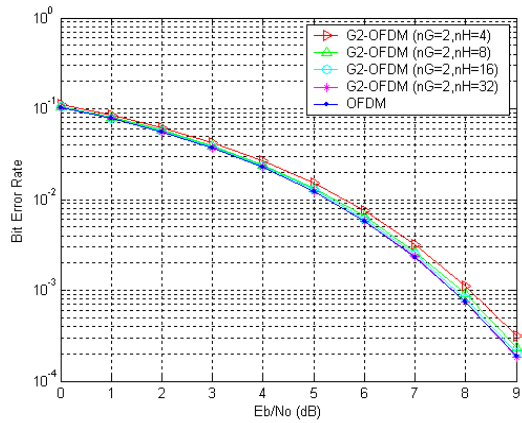
(b)



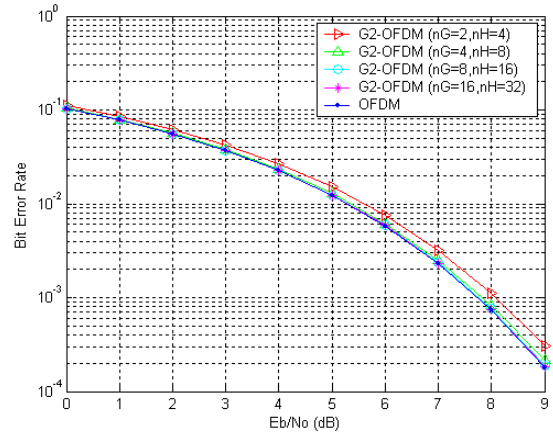
(c)



(d)



(e)



(f)

Fig. 13 BER vs E_b/N_0 for G2-OFDM, in three conditions: (a) $nG=nH$, (b), (c), (d) $nG>nH$ and (e), (f) $nG<nH$.

The BER vs E_b/N_0 performance of G2-OFDM are explained as in the following points:

1. For $nG=nH$
At a BER of 10^{-2} , the relative processing loss for G2-OFDM ($n=1$) is about 0.75 dB. The system with $n=8$ upward gives an identical performance with OFDM.
2. For $nG>nH$
G2-OFDM gives a performance identical to OFDM by using $\{nG=8, nH=16\}$ and $\{nG=16, nH=8\}$. With $\{nG=4, nH=2\}$, there is still a processing loss of about

0.00001 at BER of 10^{-3} while at a higher BER, i.e. 10^{-2} the system performance is similar to OFDM. This rule is also considered when n_G is various ($n=4,8,16$), and n_H is unchanging ($n_H=2$). Thus, the H matrix at transmitter and receiver does not greatly affect the G2-OFDM system performance when we adjust n_G to be higher than n_H .

3. For $n_G < n_H$

- (a) At a BER of 10^{-3} the relative processing loss for $\{n_G=2, n_H=4\}$ is about 0.4 dB. Then when we use $\{n_G=2, n_H=8\}$ the processing loss reduces to about 0.2 dB. The use of $\{n_G=2, n_H=16\}$ gives a gain of about 0.35 dB. Using $\{n_G=2, n_H=32\}$ the system gives identical performance to OFDM.
- (b) With $\{n_G=4, n_H=8\}$ the relative processing loss is about 0.3 dB. OFDM and G2-OFDM using $\{n_G=8, n_H=16\}$ have identical performance.

IV. CONCLUSION

G-OFDM and its variants have been proposed to reduce the complexity of OFDM. The performance of G-OFDM and its variants were examined in AWGN channels, including a discussion of the processing gain/loss and simulation results. There is a small reduction in G-OFDM performance compared to OFDM. The non-uniformity of SNR among sub-carriers mars the G system performance. The matrix transformation for both transmitter and receiver experience non-uniform row-gain, larger for some G-OFDM variants such as G1-OFDM. Using different levels of n-quantization makes it possible to trade system implementation complexity against small reductions of system performance. G-OFDM with n-level quantization adds modest complexity but push performance increasingly close to that of OFDM $n \rightarrow \infty$. Identical performance with OFDM is given by the following minimum conditions for G-OFDM and its variants: 1). G-OFDM: $n_G=8$; 2). G1-OFDM: $n_G=32$; 3). G2-OFDM: a) $n_G=n_H$: $\{n_G=n_H=8\}$, b) $n_G > n_H$: $\{n_G=8, n_H=2\}$, c) $n_G < n_H$: $\{n_G=2, n_H=32\}$ and $\{n_G=8, n_H=16\}$; 4).

REFERENCES

- [1] R. Nissel, S. Schwarz and M. Rupp, "Filter Bank Multicarrier Modulation Schemes for Future Mobile Communications," in *IEEE Journal on Selected Areas in Communications*, vol. 35, no. 8, pp. 1768-1782, Aug. 2017, doi: 10.1109/JSAC.2017.2710022.
- [2] J. Choi, "On the Error Rate Analysis of Coded OFDM Over Multipath Fading Channels," in *IEEE Wireless Communications Letters*, vol. 8, no. 2, pp. 536-539, April 2019, doi: 10.1109/LWC.2018.2878820.
- [3] NMAED Wirastuti, CCW Emehel, "Handover Scenarios for Mobile WiMAX and Wireless LAN Heterogeneous Network", *Indonesian Journal of Electrical Engineering and Computer Science* vol. 12, no. 8, 2014.
- [4] G. Bournaka, M. Ummenhofer, D. Cristallini, J. Palmer and A. Summers, "Experimental Study for Transmitter Imperfections in DVB-T Based Passive Radar," in *IEEE Transactions on Aerospace and Electronic Systems*, vol. 54, no. 3, pp. 1341-1354, June 2018, doi: 10.1109/TAES.2017.2785518.
- [5] A. Makki, A. Siddig, M. M. Saad, C. J. Bleakley and J. R. Cavallaro, "High-resolution time of arrival estimation for OFDM-based transceivers," in *Electronics Letters*, vol. 51, no. 3, pp. 294-296, 5 2 2015, doi: 10.1049/el.2014.3677.
- [6] S. R. Band, M. S. Dorle and S. S. Dorle, "BER performance of WiMAX system using wavelet packet modulation technique," *2016 World Conference on Futuristic Trends in Research and Innovation for Social Welfare (Startup Conclave)*, Coimbatore, 2016, pp. 1-5, doi: 10.1109/STARTUP.2016.7583917.
- [7] N. Sharma, I. Deb, A. Jain and B. Bhattacharyya, "Physical Layer Performance Analysis of MIMO-WiMAX on Simulink," 2018

- International Conference on Communication and Signal Processing (ICCSP), Chennai, 2018, pp. 979-983, doi: 10.1109/ICCSP.2018.8524293.
- [8] I. Lazov, "Entropy Analysis of Broadband Wireless Access Systems," in *IEEE Systems Journal*, vol. 11, no. 4, pp. 2366-2373, Dec. 2017, doi: 10.1109/JSYST.2015.2456941.
- [9] I W Widhiada, I N Budiarsa, I M Widiyarta and T Cogliatore, "Comparison of PID and fuzzy logic to control the motions of robotic prosthetic limbs", *IOP Conference Series: Materials Science and Engineering*, Volume 673, Broad Exposure to Science and Technology 2019 (BEST2019), Bali, Indonesia, doi:10.1088/1757-899X/673/1/012109.
- [10] W. Widhiada, T. G. T. Nindhia, and I. N. Budiarsa, "Design of The Bionic Robot Hand with Electromyography Smart Sensor based on MATLAB/Simulink", *International Journal of Mechanical Engineering and Robotics Research* Vol. 9, No. 8, August 2020, pp.1122-1127, doi: 10.18178/ijmerr.9.8.1122-1127.
- [11] Y. A. Al-Jawhar, K. N. Ramli, A. Mustapha, S. A. Mostafa, N. S. Mohd Shah and M. A. Taher, "Reducing PAPR With Low Complexity for 4G and 5G Waveform Designs," in *IEEE Access*, vol. 7, pp. 97673-97688, 2019, doi: 10.1109/ACCESS.2019.2930121.
- [12] I. Selinis, K. Katsaros, M. Allayioti, S. Vahid and R. Tafazolli, "The Race to 5G Era; LTE and Wi-Fi," in *IEEE Access*, vol. 6, pp. 56598-56636, 2018, doi: 10.1109/ACCESS.2018.2867729.
- [13] K. Jallouli, M. Mazouzi, A. B. Ahmed, A. Monemi and S. Hasnaoui, "Multicore MIMO-OFDM LTE Optimizing," *2018 International Conference on Internet of Things, Embedded Systems and Communications (IINTEC)*, Hammamet, Tunisia, 2018, pp. 166-170, doi: 10.1109/IINTEC.2018.8695290.
- [14] N. M. A. E. D. Wirastuti, Ni Putu Lintang Anggitiadewi, Nyoman Pramaita, "Pulse shaping methods for inter carrier interference reduction in OFDM system", *Telkomnika*, vol. 18, no. 5, pp. 2276-2283, 2020, doi: http://dx.doi.org/10.12928/telkomnika.v18i5.13840.
- [15] S. J. Shepherd et al., "A Lower Complexity Discrete Fourier Transform", *Mathematics Today*, vol. 39, no. 5, pp. 150-156, October 2003.
- [16] S. J. Shepherd et al., "The Very Fast Fourier Transform ~ A Tool for Science in the 21st Century," *ICTAA Conference*, 2004.
- [17] D. L. Rani, M. Bharathi and N. Padmaja, "Performance Comparison of FFT, DCT, DWT and DDDWT-OFDM in Rayleigh Channel," *2019 International Conference on Smart Systems and Inventive Technology (ICSSIT)*, Tirunelveli, India, 2019, pp. 392-394, doi: 10.1109/ICSSIT46314.2019.8987953.
- [18] Mannan and A. Habib, "Adaptive processing of image using DWT and FFT OFDM in AWGN and Rayleigh channel," in *2017 International Conference on Communication, Computing and Digital Systems (C-CODE)*, Islamabad, 2017, pp. 346-350, doi: 10.1109/CCODE.2017.7918955.
- [19] J. Lee and H. Ryu, "Design and Comparison of Discrete Wavelet Transform Based OFDM (DWT-OFDM) System," in *2018 Tenth International Conference on Ubiquitous and Future Networks (ICUFN)*, Prague, 2018, pp. 881-885, doi: 10.1109/ICUFN.2018.8437028.
- [20] M. S. Sheela, T. P. Surekha, and K. R. Arjun, "Analysis of BER in OFDM using Wavelet and FFT based Method," in *2017 International Conference on Current Trends in Computer, Electrical, Electronics and Communication (CTCEEC)*, Mysore, 2017, pp. 473-476, doi: 10.1109/CTCEEC.2017.8455191.
- [21] S. Baig, H. Muhammad Asif, T. Umer, S. Mumtaz, M. Shafiq, and J. Choi, "High Data Rate Discrete Wavelet Transform-Based PLC-VLC Design for 5G Communication Systems," *IEEE Access*, vol. 6, pp. 52490-52499, 2018, doi: 10.1109/ACCESS.2018.2870138.
- [22] Ni Made Ary Esta Dewi Wirastuti, Ida Bagus Dharma Dhyaksa, "Transformasi Wavelet dengan Teknik Clipping Filtering untuk Mereduksi PAPR pada OFDM", *Jurnal Teknik Elektro* Vol. 12 No. 1 7 Januari - Juni 2020.
- [23] M. Chaffi, J. P. Coon and D. A. Hedges, "DCT-OFDM With Index Modulation," in *IEEE Communications Letters*, vol. 21, no. 7, pp. 1489-1492, July 2017, doi: 10.1109/LCOMM.2017.2682843.
- [24] C. He, A. Cao, L. Xiao, L. Zhang, P. Xiao and K. Nikitopoulos, "Enhanced DCT-OFDM System With Index Modulation," in *IEEE Transactions on Vehicular Technology*, vol. 68, no. 5, pp. 5134-5138, May 2019, doi: 10.1109/TVT.2019.2893684.
- [25] Zhenlei Zhou, Bangjiang Lin, Xuan Tang, Sushank Chaudhary, Chun Lin, and Haiguang Zhang "Performance comparison of DFT-OFDM, DCT-OFDM, and DWT-OFDM for visible light communications",

- Proc. SPIE 11048, 17th International Conference on Optical Communications and Networks (ICOON2018), 1104822 (14 February 2019); <https://doi.org/10.1117/12.2522838>.
- [26] Z. A. Abbas, N. B. Sulaiman, N. A. M. Yunus, W. Z. Wan Hasan and M. K. Ahmed, "An FPGA implementation and performance analysis between Radix-2 and Radix-4 of 4096 point FFT," 2018 IEEE 5th International Conference on Smart Instrumentation, Measurement and Application (ICSIMA), Songkla, Thailand, 2018, pp. 1-4, doi: 10.1109/ICSIMA.2018.8688777.
- [27] M. Patrikar and V. Tehre, "Design and power measurement of different points FFT using Radix-2 algorithm for FPGA implementation," 2017 International conference of Electronics, Communication and Aerospace Technology (ICECA), Coimbatore, 2017, pp. 190-195, doi: 10.1109/ICECA.2017.8203669.
- [28] P. P. Vinchurkar, S. V. Rathkanthiwar and S. M. Kakde, "HDL Implementation of DFT Architectures Using Winograd Fast Fourier Transform Algorithm," 2015 Fifth International Conference on Communication Systems and Network Technologies, Gwalior, 2015, pp. 397-401, doi: 10.1109/CSNT.2015.147.
- [29] N. M. A. E. D. Wirastuti, J. M. Noras and S. M. R. Jones, "Evaluation of the very fast fourier transform applied to OFDM," 2005 The 2nd IEE/EURASIP Conference on DSPEnabledRadio (Ref. No. 2005/11086), London, UK, 2005, pp. 12-12/6, doi: 10.1049/ic:20050382.